*Semiconductor Physics, Quantum Electronics & Optoelectronics, 2025. V. 28, No 4. P. 432-440.*

*Semiconductor physics*

# Thermodynamic and kinetic processes of modifying cadmium telluride-based heterosystems initiated by nanosecond intense laser radiation

**S.M. Levytskyi**

*V. Lashkaryov Institute of Semiconductor Physics, NAS of Ukraine, Kyiv, Ukraine*
*E-mail: levytskyism@gmail.com*

**Abstract.** The paper considers the mechanisms of mass transfer in an In/CdTe system under nanosecond pulsed laser irradiation, which are caused by nonstationarity, nonequilibrium, physical and geometric nonlinearity, high rate and simultaneity of various physical processes. Moreover, threshold processes such as phase transitions and ablation in the metal/CdTe heterosystem, under powerful nanosecond laser irradiation at normal conditions and in a liquid medium are analyzed. The melting and ablation thresholds under nanosecond laser irradiation of the metal (In)/CdTe film structures in water are found and their change due to appearance of nonlinearities (caused by changes in the physical characteristics of In) and pressure generation is studied. It is found out that the pressure in the energy release region under irradiation of the In/CdTe with a neodymium laser ($\tau_{pulse}$ = 7 ns) in water is 17 times greater in the case of the photothermoacoustic effect and 90 times greater in the case of indium melting.

**Keywords:** CdTe, In/CdTe, pulsed laser irradiation, photothermoacoustic effect, doping, melting.

https://doi.org/10.15407/spqeo28.04.432
PACS 61.46.Df, 61.72.uf

Manuscript received 11.09.25; revised version received 16.11.25; accepted for publication 26.11.25; published online 15.12.25.

## 1. Introduction

Nanosecond laser irradiation of In/CdTe film structures is one of the promising methods for forming shallow and sharp *p-n* junctions, *e.g.* for creating diodes for CdTe-based ionizing radiation detectors. This method implements a non-thermal barodiffusion mechanism for introducing an In impurity into CdTe due to sharp pressure gradients [1–6].

One of the important issues of this method is formation of defects in the diffusion zone of the semiconductor, since the energy density of the laser pulse $E_s$ must be increased to increase the diffusion coefficient and concentration of electrically active doping atoms. This problem may be effectively avoided by using an irradiation method in liquids transparent to laser radiation (*e.g.* water) to clamp the outer face. In this case, sharp pressure gradients can be provided at smaller $E_s$, thus avoiding significant heating and, hence, defect formation.

However, this improvement of the technique requires *in-situ* control of the pressure value during the processes of melting, ablation and water vaporization, since the pressure can increase by an order of magnitude when $E_s$ changes by only 10…20%. It is convenient to use the photothermoacoustic (FTA) phenomenon accompanying these processes and, accordingly, the FTA method [7, 8].

Multiple irradiation in water at low energies is also promising. In this case, current-voltage characteristics of the In/CdTe/Au structures are measured to verify laser-stimulated diffusion.

This work presents experimental studies supported by theoretical calculations of pressure generation during modification of heterosystems based on cadmium telluride in water, initiated by nanosecond intense laser radiation. The melting threshold of indium during irradiation of In/CdTe in water is determined by the FTA method.

## 2. Experimental methodology

*p*-CdTe crystals with dimensions of 5×5×0.5..3 mm and a resistivity of $(2…4)\cdot10^9$ Ohm·cm were cut along the (111) orientation. Before deposition of In film, the surface was chemically polished. The In film with a thickness of 400 nm as well as additional In and Au contacts for measuring current-voltage characteristics were deposited using thermal spraying in vacuum at a pressure of $10^{-5}$ atm.

The obtained In/CdTe structures were irradiated with pulses of neodymium YAG:Nd (λ = 532 nm, 2nd harmonic, $\tau_{pulse}$ = 7 ns) and ruby (λ = 694 nm, $\tau_{pulse}$ = 20 ns) lasers. A homogenizer was used to evenly distribute the intensity over the sample surface, while the inhomo-

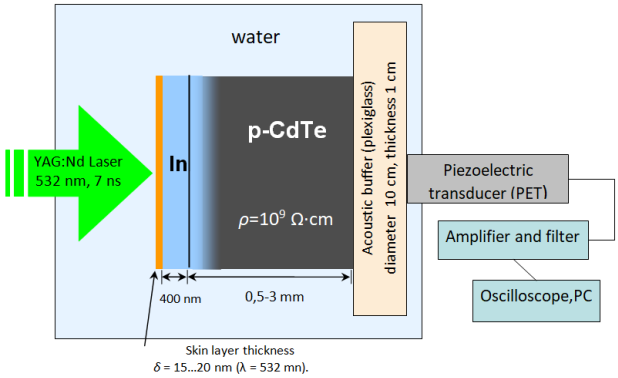


**Fig. 1.** Scheme of the experiment on irradiation in water by using the photothermoacoustic method.

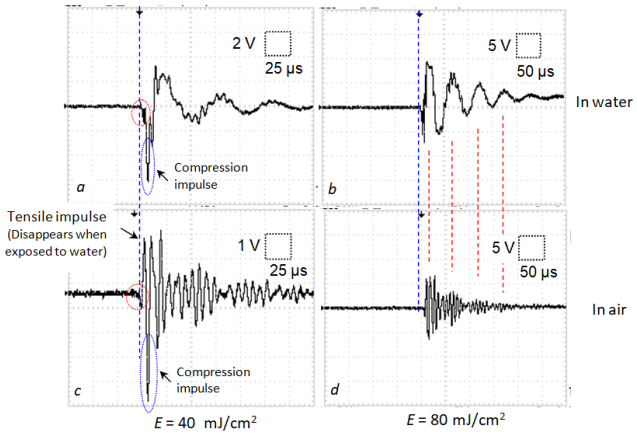


**Fig. 2.** Acoustic responses to neodymium laser irradiation of In/CdTe in water and air. Piezosensor 20…200 kHz.

geneous part of the beam was cut out. The samples were irradiated in distilled deionized water (Fig. 1) and under normal conditions in air.

Fig. 1 shows the scheme of the experiment on irradiation and recording of acoustic response. The acoustic signals were measured using piezosensors, amplified and fed to an oscilloscope and computer. The frequency ranges of ultrasound measurements were $\Delta f$ = 20…200, 200…500, 1000…2000, and 500…1000 kHz. The total gain of the electrical signals of the acoustic response was 40…74 dB. In this dynamic range, the gain of the electrical signals ($A_{out}/A_{in}$) was linear.

A sample on a Plexiglas substrate and a piezoelectric transducer (PET) were located in a grounded copper cell (cuvette) filled with water. The geometry of the cell and the substrate was calculated so to separate the first and second pulses in time and eliminate the so-called "acoustic echo" from the first (useful) pulse. The shape, duration and amplitude of the laser and acoustic pulses were measured using Tektronix TDS 1012 (100 MHz) and TDS 2022 V (200 MHz) recording oscilloscopes. The absorption coefficient of the input glass and water at the wavelength of 532 nm was 11%. This technique allowed one to measure threshold processes and to estimate the pressure values in the irradiation zone.

The laser plasma flash was also recorded by a camera with OS 14 and KS 11–19 type filters used for cutting out the laser radiation. The morphology of the crystal surface before and after the irradiation was studied using a MI-9 optical microscope.

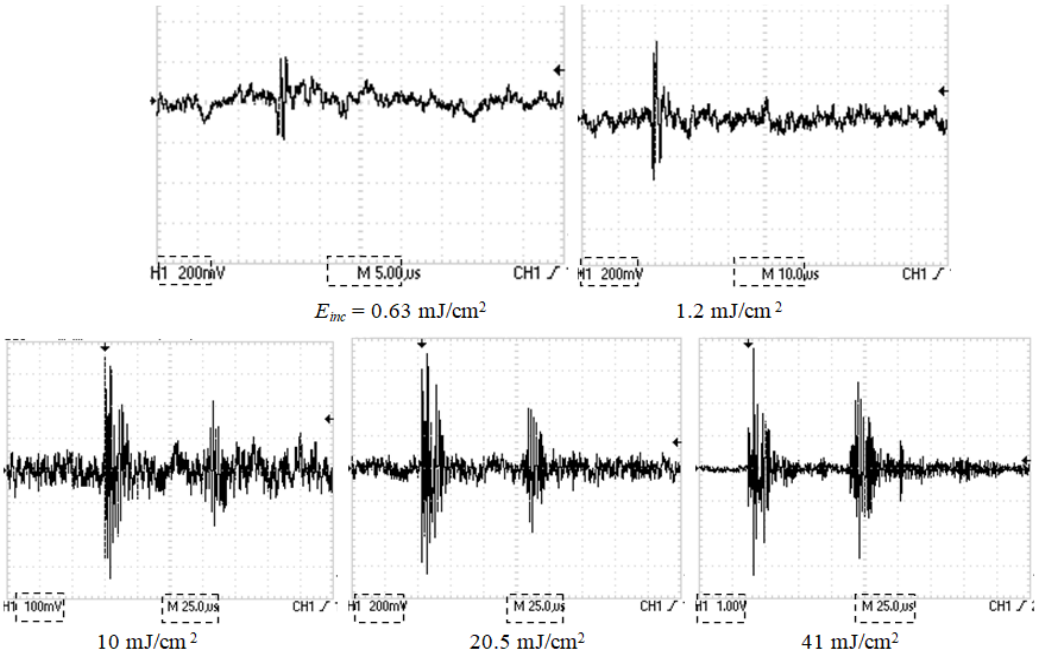


**Fig. 3.** A series of acoustic signals during irradiation of In/CdTe with a neodymium laser at various energies $E_{inc}$, mJ/cm$^2$. $\tau_{pulse}$ = 7 ns. Piezosensor 200…2000 kHz.

### 3. Experimental results

Fig. 2 shows typical signals in the frequency range of 20 to 200 kHz from In/CdTe irradiated with a neodymium laser at two energy values in water and in air, recorded using a piezosensor. The gain coefficients are 68…70 dB in water and 72…74 dB in air. It can be seen from this figure that in the case of irradiation in water, the signal is somewhat modulated due to damping of the sample surface by water. That is, the recoil impulse is very weakly manifested due to clamping of the face, since the coefficient of isothermal comprehensive compression of water $-1/V \cdot (dV/dP)$ is very small, $51.1 \cdot 10^{-11}$ Pa$^{-1}$ (0 °C).

Fig. 3 shows characteristic acoustic signals in the frequency range of 200 to 2000 kHz obtained at increasing the laser pulse energy $E_{inc}$, recorded using a piezosensor. Here, the second pulse also corresponds to reflection from the lateral (diagonal) face of the buffer. The frames below indicate the scale divisions (V/division, μs/division).

Here, the amplitude and duration of the signal linearly increase at increasing $E_{inc}$.

Fig. 4 shows the amplitude-frequency characteristic (AFC) of the acoustic signal during nanosecond irradiation of In/CdTe (a) and the AFC of the noise (background) signal in the absence of irradiation (b) for comparison. It can be seen from this figure that the AFC spectrum of the FTA signal is wide – 2.5 MHz. The maximum at 500 kHz corresponds to the resonant frequency of the piezosensor.

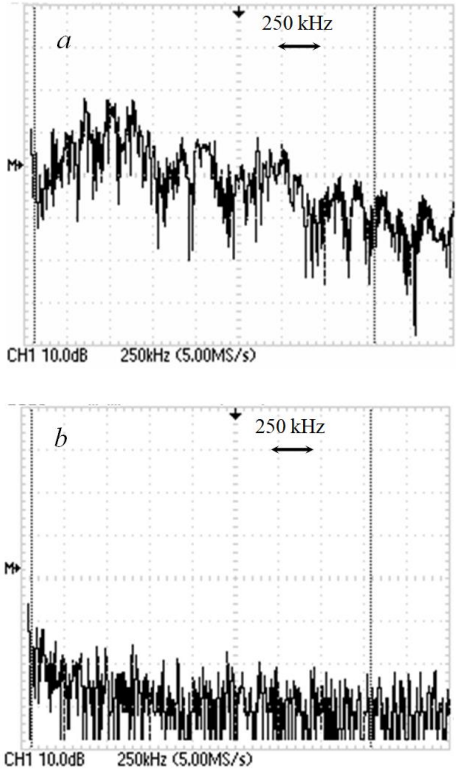


**Fig. 4.** Amplitude-frequency characteristic of the acoustic response during irradiation of In/CdTe at $E$ = 28.7 mJ/cm$^2$ (a) and AFC of the inherent noise of the equipment (b).

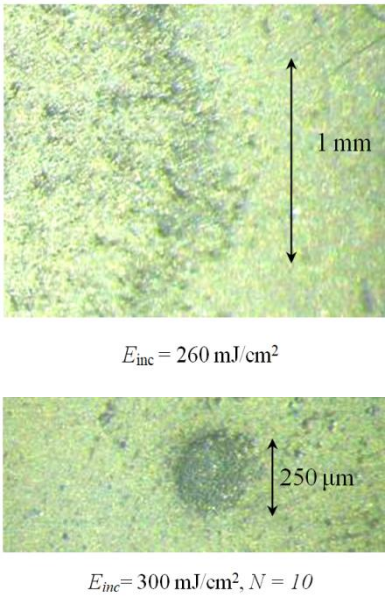


**Fig. 5.** Micrograph of the surface of the In/CdTe structure after irradiation with a neodymium laser ($\tau_{pulse}$ = 7 ns).

Fig. 5 shows the surface of the In/CdTe film after laser irradiation at relatively large $E_{inc}$. It can be seen from Fig. 5a that melting and partial ablation of indium occurred causing appearance of so-called erosion craters, the depth of which reached the CdTe surface. The indium film completely disappears by irradiation with 10 pulses at $E_{inc}$ = 300 mJ/cm$^2$. A part of In diffuses and mixes with CdTe, and the ablation products dissolve in water (Fig. 5b).

As follows from these images, the given energies are not effective for doping CdTe with indium, since intensive defect formation occurs. When irradiating in water, one should take into account water vaporization – a well-known phenomenon of the so-called "explosive" evaporation of water during nanosecond laser irradiation of metals [9]. It is clear that this process is fundamentally different from the usual evaporation of water at temperatures reaching 100 °C. First, vapors practically do not have time to form at such times (nanoseconds). Second, the boiling point of water shifts to higher temperatures due to significant pressures in the irradiation zone. A superheated liquid-vapor layer is formed [9, 10].

#### 3.1. Determination of melting threshold and pressure during irradiation of In/CdTe in water with a neodymium laser by using the FTA method

Fig. 6 shows the dependences of the acoustic response amplitude on the laser pulse energy density $A(E_{inc})$ upon irradiation of the In (400 nm) / CdTe system in distilled deionized water (a) and in air under normal conditions (b). For comparison, the dependence (4 points in Fig. 6a) for GaAs is also presented. It can be seen from this figure that the slope of the curve upon irradiation of the structure in water increases starting from the value of 80 mJ/cm$^2$, upon irradiation in air – starting from the value of 115 mJ/cm$^2$ (within the discreteness of the neutral filter selection, *i.e.* melting begins at ≈110 mJ/cm$^2$).

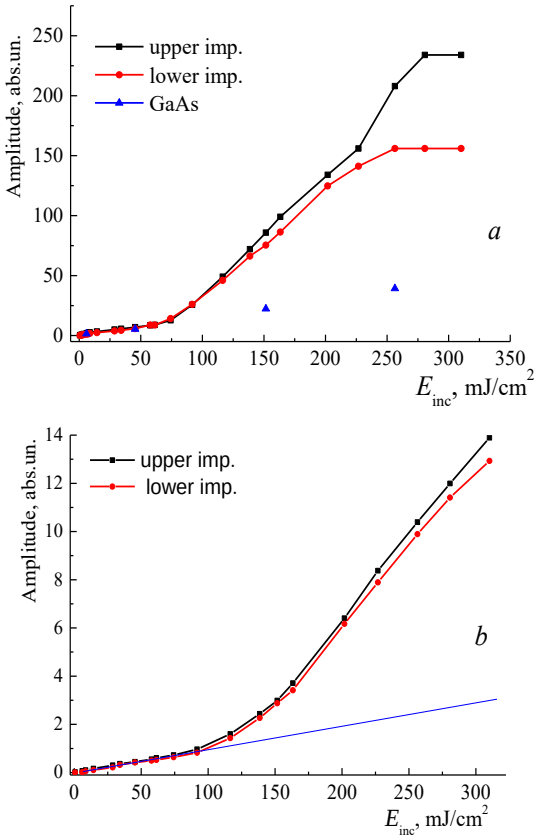


**Fig. 6.** Amplitude of acoustic response *versus* energy density of a neodymium laser pulse (7 ns) upon irradiation of In (400 nm) / CdTe in water (a) and air (b). The upper curve is the positive maximum pulse and the lower curve is the negative pulse (signals in Fig. 3).

The graph takes into account the absorption from the glass and water in the cuvette (11%), *i.e.* $E_{inc}$ is the energy incident on the In surface with an area *S*. The beginning of the increase of the slope corresponds to the melting threshold of the indium film. The melting threshold is somewhat lower for irradiation in water. On the one hand, due to the influence of pressure, the melting point of In in the *T*(*P*) dependence (Fig. 8) increases. On the other hand, the accompanying process of indium ablation makes a significant contribution in these two cases. The indium ablation takes place in a different way for irradiation in water. The ionized atoms do not create a plasma cloud upon reaching the melting threshold and, hence, no laser breakdown is observed. This process begins only at $E_{inc}$ = 160 mJ/cm$^2$.

Appearance of a characteristic plasma glow was recorded using a camera. Up to this value of $E_{inc}$, there was no flash, and the ablation products dissolved in water. Appearance of a bubble at the irradiation site was observed above 160 mJ/cm$^2$. At irradiation in air, melting was accompanied by intense ablation, which is a probable reason why the dependence in Fig. 6b in the region $E$ = 110…165 mJ/cm$^2$ is similar to an exponential one.

Since a significant (for example, up to 200 °C) increase in $T_{melt}$ occurs at a pressure of $10^9$ Pa, which is two orders of magnitude lower than the pressure values that we have registered and calculated (see below), the decrease in the melting threshold of a 400-nm indium film is explained by the absence of ablation in water. Due to ablation in air, the surface is significantly cooled. The heat flow from the In surface can be written as $Q = L_{\text{In}} J_{\text{In}}$, where $J_{\text{In}}(T) = 0.435 P_{vapor}(T)\sqrt{\frac{M}{2\pi k_B T}}$ is the flow density of mass of evaporated atoms, *M* is the mass of an atom, and $L_{\text{In}}$ is the latent heat of evaporation of indium [11, 12], respectively. This leads even to that the beginning (threshold) of melting of semiconductors under nanosecond irradiation does not occur on the surface but at a certain depth from the surface. The temperature difference (between the surface and the depth of the sample, where laser-induced doping occurs) can be 100…150 °C [12]. Given the low $T_{melt}$ of In, the contribution of ablation to the melting threshold of In in the In/CdTe structure is significant. Estimation of the heat flow and temperature showed that such cooling of the surface of the In film occurs at ~20 °C.

Before melting, the pressure amplitude is proportional to the intensity of the laser radiation. It is also proportional to the absorbed energy of laser radiation when passing through the melting threshold. This is also true for a mechanically clamped surface with a dielectric [13]. This is because the FTA pressure and the substance vapor pressure fundamentally differ in their manifestation depending on the rate of heat release. Such difference is due to that the former pressure is mainly defined by the intensity of light, while the latter one is defined by the input energy [10, 14]. We also note that the linear dependences *A*(*I*) of the thermo-optical and evaporative acoustic pulses during nanosecond irradiation of water have different slopes [15].

During laser exposure, the parameters of indium and the adjacent water layer (coefficients of light absorption, thermal conductivity, *etc.*) can change, which leads to thermal nonlinearity [10, 13, 14, 15]. For example, during stepwise shock compression in the pressure range up to 27 GPa at temperatures up to 1000 K, the thermal conductivity coefficient of indium does not depend on temperature, and its threefold increase is caused by only the change in the volume during compression [16].

When GaAs is irradiated with a neodymium laser, the amplitude is smaller (Fig. 6a). According to [17], the theoretically calculated melting threshold of GaAs under normal conditions at $\tau_{pulse}$ = 7 ns is $E_{inc}$ = 250…280 mJ/cm$^2$ (at $R$ = 0.37).

The saturation in Fig. 6a is already caused by reaching the limit of the dynamic range at a given amplification of electrical signals.

Comparative experiments have established that the amplitude *A* of the photothermoacoustic signal during irradiation in water is 15…17 times greater than that during irradiation in air. Since *A* is proportional to the transverse component of deformation and, hence, compression, $P_{water}/P_{air}$ = 15…17. Moreover, $P_{water}/P_{air}$ = 90…100 in the entire region after the melting threshold.

### 3.2. Calculation of pressure during nanosecond irradiation of In/CdTe in water

The pressure value $\Delta P_{melt}$ due to change in the density $\Delta\rho_{In} = \rho_{solidphase} - \rho_{melt}$ during melting is determined from a linear approximation with respect to $\Delta\rho_{In}$ according to the following expression [18, 19]:

$$\Delta P_{melt} = \Delta\rho_{In}\, d(Vh)/dt\,, \qquad (1)$$

where $V$ is the rate of change of the thickness of the melt layer $h$. In fact, the value $\Delta P_{melt}$ quadratically depends on the maximum value of $V$ [18, 19] and increases with the increase in the difference $\Delta\rho_{In}$. In our case, $V$ depends very weakly on time. This is shown below in paragraph 5 with reference to the results of mathematical modeling of the melt depth. The value $V = dh/dt$ is calculated to change from 5.47 to 80.6 m/s when $E$ changes from 80 to 310 mJ/cm$^2$, and has a close to logarithmic dependence (Fig. 7a).

Fig. 7b also shows the dependence of the density of In in the molten state [20]. It can be seen from this figure that $\Delta\rho_{In}$ decreases during melting and heating, *i.e.* the volume increases.

According to the simulations, the propagation speed of the melting front $V$ for CdTe being irradiated with an excimer KrF laser at $\tau_{pulse}$ = 20 ns in air is 2.7…5 m/s at $E_{abs}$ = 5…100 mJ/cm$^2$ [11]. Irradiation with a CdTe ruby laser at $\tau_p$ = 80 ns makes melting begin at the depth of

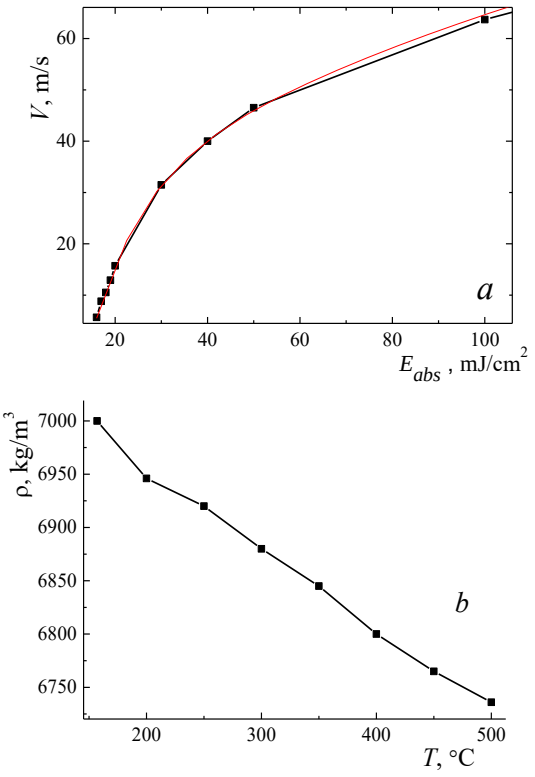


**Fig. 7.** (a) Dependence of the speed of the melt-solid phase front of an indium film at $h_{In}$ = 400 nm upon irradiation of In/CdTe with a neodymium laser ($\tau_{pulse}$ = 7 ns). (b) Dependence of the density of liquid indium phase on temperature.

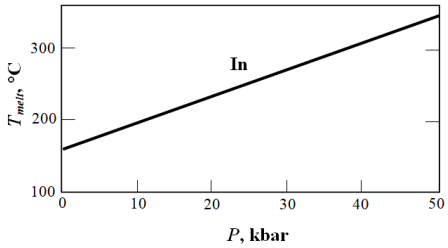


**Fig. 8.** Pressure dependence of the melting point of In.

19.5 nm. The speed of the melt front moving deep in the sample equals as 2.5 m/s, and the speed of moving to the surface is 1.5 m/s at $E_{abs}$ = 100…300 mJ/cm$^2$ [12]. When GaAs is irradiated with a ruby laser at $\tau_{pulse}$ = 70 ns, $V$ = 5.4 m/s at $E_{abs}$ = 1000 mJ/cm$^2$ [21]. When Si is irradiated with a ruby laser at $\tau_{pulse}$ = 70 ns, $V_{melt}$ = 8…9 m/s and $V_{crystalliz}$ = 3…4 m/s at $E_{abs}$ = 1.5…2 mJ/cm$^2$ [22]. At $\tau_{pulse}$ = 32 ns, $V$ = 6…8 m/s at $E_{abs}$ = 190…700 mJ/cm$^2$ [23].

Note that the deformation rate during melting due to volume change $\varepsilon = \dfrac{\Delta h/h_0}{\tau_{pulse}}$ calculated by us is also of the order of $10^6$ s$^{-1}$ (similar to [1, 2]), *i.e.*, it is proportionate to the deformation rate during the FTA effect.

In the conditions of a clamped face, the mechanism of pressure increase due to abrupt expansion of In is practically dominant (critical). Therefore, the shift of the melting point with pressure should be taken into account. This dependence is shown in Fig. 8.

It is also clear that during nanosecond laser irradiation, there is a certain increase in the boiling point of water due to instantaneous increase in pressure in the irradiation area. For example, $T_{boil}$ = 180 °C at $P$ = 1000 kPa.

For example, when mercury clamped with a quartz plate is irradiated with a nanosecond (6 ns) laser, the threshold energy density, at which boiling begins, is almost twice as high and amounts to 81 mJ/cm$^2$. In this case, the maximum surface temperature will exceed 700 °C, which is almost twice the boiling temperature [10].

In the case of the FTA signal with a clamped face, the pressure was calculated using the following expressions [10, 14]:

$$p_{\max}(x=0) = \frac{AI_{inc}\beta_T c}{(N+1)C_p} \qquad (2)$$

and [8]

$$p_{\max}(x=0) = \frac{\alpha c^2 \beta_T A E_{inc}}{2C_p}\frac{1-N}{1+N}\,. \qquad (3)$$

Here, the ratio of the indium and water impedances $N = \rho_{In}\upsilon_{In}/\rho_{water}\upsilon_{water}$ = 7.6 is taken into account. Furthermore, $\beta_T$ is the coefficient of volumetric thermal expansion, $c$ is the velocity of elastic waves, $C_p$ is the heat capacity, and $R$ is the optical reflection coefficient, respectively. Under normal conditions, without taking into account the processes of defect formation, melting and ablation, the magnitude of shear (transverse,

**Table 1.** Physical parameters of indium.

| Speed of sound (longitudinal mode) $c_l$, m/s | Density ρ, kg/m$^3$ | Absorption coefficient $\alpha_\lambda$ = 0.532 m$^{-1}$ | Reflection coefficient $R$ | Coefficient of linear thermal expansion $\alpha_T$, 1/deg (293…333 K), ($\beta_T = 3\cdot\alpha_T$) | $T_{melting}$ °C |
|---|---|---|---|---|---|
| 1400 | 7310 | $6\cdot10^7$ | 0.8 | $3.3\cdot10^{-5}$ | 157 |
| | | | | | |
| Heat capacity $C_P$, J/kg·deg | Thermal conductivity χ, m$^2$/s | Thermal conductivity λ, J/m·s·deg | Elasticity modulus $E$, Pa | Shear modulus $G$, Pa | Poisson's ratio ν |
| 234.46 | $5.0761\cdot10^{-5}$ | 87 | $1.1\cdot10^{10}$ | $4\cdot10^9$ | 0.46 |

tangential) strain is determined as $\sigma = \alpha_T G \Delta T (1-\nu)^{-1}$, where $\alpha_T$ is the linear thermal expansion coefficient, $G$ is the shear modulus, $\Delta T$ is the temperature increase upon irradiation, and ν is the Poisson ratio, respectively.

The physical parameters of In are given in Table 1. Using the expressions (1)–(3), the dependence of the pressure on $E_{inc}$ of the laser (Fig. 9) was theoretically calculated. It can be seen from Fig. 9 that the pressure increase due to melting (Eq. (1)) is proportional to the FTA signal (Eqs (2) and (3)), while the dependence above 80 mJ/cm$^2$ becomes nonlinear. This dependence is similar to the dependence shown in Fig. 6, but with the following differences: the slope of the experimental curve after the melting threshold is greater, and possible ablation and instantaneous boiling of water are not taken into account theoretically.

Therefore, since exact mathematical calculation of the pressure value during melting and related processes is quite complicated, the pressure was calculated in the region of small values of the FTA signal. For this case, the expressions are simple and contain no nonlinear distortions. Since the amplifier characteristic was linear in the amplitude range of 0.1 mV to 5 V, the pressure value in this region could be determined.

The deformation rate during melting is proportional in the linear approximation to the amplitude of the FTA signal, which determines the course of the dependence in Fig. 9. We note here that the pressure $P$ refers to the irradiation zone with the volume $S\cdot l_t$, where $l_t$ is the depth of thermal diffusion.

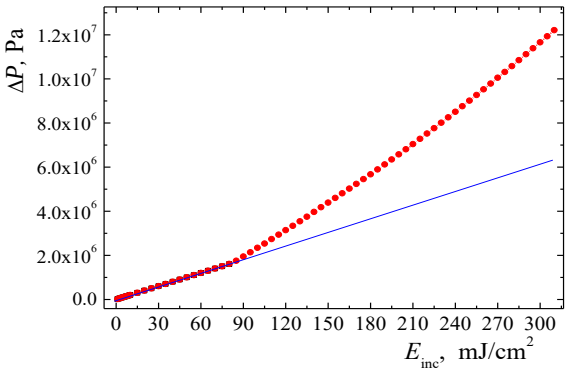


**Fig. 9.** Dependence of the pressure increase on the In film surface $\Delta P$ during laser irradiation of In/CdTe with a neodymium laser ($\tau_{pulse}$= 7 ns) in water.

The amplitude (potential at the piezoelectric element electrodes) of the photothermoacoustic response is given by the expression $\tilde{U} \sim \int_0^h \frac{\alpha_T E_Y \tilde{T}}{(1-\nu)} dz$ [24]. Here, $\alpha_T(T)$ is the thermal expansion coefficient, $E_Y$ is the Young's modulus, which can be the modulus of elastic constants in specific cases for certain modes and crystal orientations, ν is the Poisson ratio, and $\tilde{T}$ is the variable component of temperature, in fact $dT/dt$, respectively. The amplitude is proportional to the magnitude of the temperature change and the magnitude of the deformation change as well as inversely proportional to the duration of the laser pulse.

The so-called "shock" deformation and generation of a pressure pulse (compression) during nanosecond irradiation in the case of the FTA effect is described by the deformation rate $\varepsilon_{zz} = \frac{1+\nu}{1-\nu}\cdot\frac{\alpha_T \Delta T}{\tau_{pulse}}$ [2]. At $\tau_{pulse}$ = 7 ns and $\Delta T$ = 500…1000 °C, $\varepsilon_{zz} = (6..12)\cdot10^6\ s^{-1}$ for In (ν = 0.46). The amplitude of the FTA signal is also proportional to the gradient of $T$ (and, hence, grad $P$).

### 3.4. Change in electrical properties of In/CdTe structures after nanosecond laser irradiation in water

A significant enhancement of rectifying properties after nanosecond laser irradiation of In/CdTe in water compared to irradiation in air is also indicated by changes in the current-voltage characteristics (CVC). Fig. 10 shows CVC of the In/CdTe/Au structure in the initial state (curve *1*) and after a single irradiation at $E$ = 100 mJ/cm$^2$ from the side of indium with a thickness of 400 nm with a neodymium laser in air (curve *2*) and in water (curve *3*). The type of CVC after the irradiation indicates enhancement of the rectifying properties of the In/CdTe contact and formation of a diode structure, which evidences doping of the CdTe surface layer with indium and formation of a *p-n* junction, similar to [1]. The leakage current at the reverse voltage decreased.

It can be seen from Fig. 10 that the rectification voltage became lower (3 V) during irradiation in water than during irradiation in air (17 V).

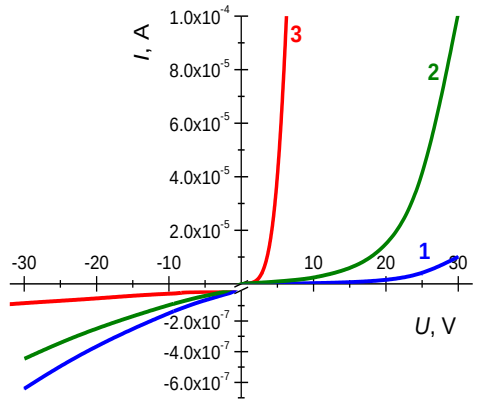


**Fig. 10.** Current-voltage characteristics of the In/CdTe/Au structure before (*1*) and after irradiation at $E_{inc}$ = 100 mJ/cm$^2$ in air (2) and in water (3).

Fig. 11 presents CVC of the In/CdTe/Au structure in the initial state (curve *1*) and after irradiation with 5 pulses (curve *2*) and 10 pulses from the side of indium with a thickness of 400 nm with a neodymium laser in water. A decrease in the rectification voltage for this irradiation method is observed. Further irradiation does not lead to an enhancement of the rectification properties, while the leakage current can already increase above 15 V (curve *3*, Fig. 11). We also observed a decrease in the rectification voltage and the leakage current upon irradiation up to 100 times at lower $E_{inc}$. In the described cases, the noise level of this detector structure will decrease.

Since the diffusion length of carriers during injection from the contact is greater than the thickness of the doped layer, the Schottky contact can play a dominant role in the current transfer mechanisms – the Schottky barrier height may decrease. However, the height of the Schottky barrier (*p*-CdTe – In) is 1.1 eV, the barrier height of the *p-n* junction $\Phi_{p\text{-CdTe}} - \Phi_{n\text{-CdTe}}$ = 5.03 – 4.43 eV = 0.6 eV, and the barrier height of the *n*-CdTe – In contact equals as 0.57 eV, *i.e.* 2 times smaller. Therefore, the *p-n* junction plays the main role in current transfer, since the rectification voltage on the direct CVC is significantly reduced being proportional to the higher barrier value.

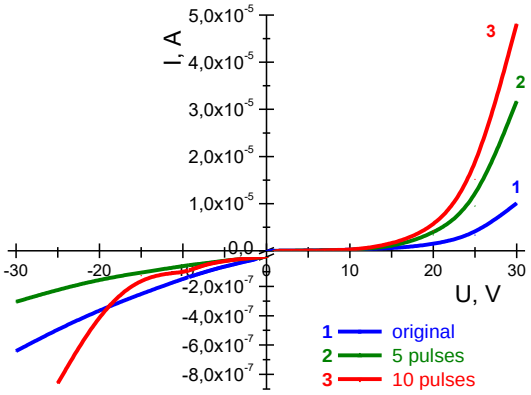


**Fig. 11.** Current-voltage characteristic of the In/CdTe/Au structure before (*1*) and after (*2* and *3*) multiple irradiation with a neodymium laser in water at $E_{inc}$ = 160 mJ/cm$^2$.

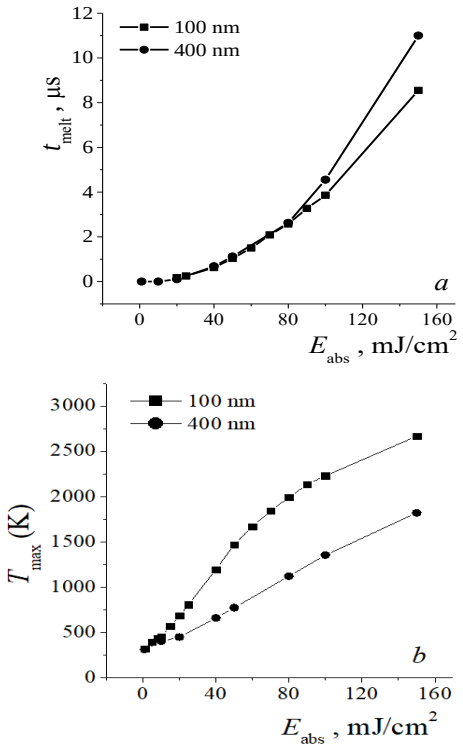


**Fig. 12.** Lifetime of the melt (a) and maximum temperature on the In/CdTe surface (b) *versus* absorbed energy density $E_{abs}$.

### 3.5. Heating and melting of In film (400 nm) / CdTe system under nanosecond laser irradiation

To unveil the features of pressure generation, the dynamics of heating and melting of the In/CdTe structure under irradiation with a ruby laser ($\tau_{pulse}$ = 20 ns) was modeled based on numerical solving of the Stefan problem. The thickness of the In film was 400 nm. The change in the surface temperature $T(t)$ under irradiation of the In film (400 nm) / CdTe system (practically semi-limited) for different values of the absorbed energy $E_{inc}$ (mJ/cm$^2$) can be calculated as $E_{abs}/(1 - R_{In})$.

The In film is heated almost uniformly in depth. The depth of the heated CdTe near-surface layer is 400…450 nm. In is characterized by a low melting point and a small latent heat of melting as compared to CdTe.

CdTe has low thermal conductivity and a higher melting point. This leads to generation of large $T$ and $P$ gradients in the near-surface layer of the semiconductor. At this, the film melts almost instantly and then remains in molten state for a long time (Fig. 12).

It was established by mathematical modeling similar to [1] that the In film with a thickness $h_{In}$ = 400 nm begins to melt at $E_{abs}$ = 16 mJ/cm$^2$. Fig. 12b shows that at $E_{abs}$ = 40 mJ/cm$^2$, the maximum temperature is $T_{max}$ = 660 K. It was found out that CdTe begins to melt (1365 K) at approximately $E_{abs}$ = 50 mJ/cm$^2$ for an In thickness of 100 nm and at $E_{abs}$ = 100 mJ/cm$^2$ for a thickness of 400 nm. Taking into account the optical reflection coefficient of indium $R$ = 0.8, $E_{inc}$ will be 250 and 400 mJ/cm$^2$, respectively. That is, barodiffusion in CdTe occurs in the solid phase in our case.

The substrate remains in the molten state 10 times less time than the film. The film is in the molten state for more than 1…10 μs (Fig. 12a), while the substrate is ten and hundreds of nanoseconds. The lifetime of the molten state of the In film at $E_{abs}$ = 40 mJ/cm$^2$ is 590, 620, and 680 ns at the film thickness $h_{In}$ = 30, 100, and 400 nm, respectively. At 100 mJ/cm$^2$ this time is 4020, 3870, and 4560 ns at the film thickness $h_{In}$ = 30, 100, and 400 nm, respectively. From the dependences $d(t)$ in Fig. 12b, the value of the melt front propagation speed $V$ is simply calculated as $V = d(d)/dt$.

It can be seen that the theoretically calculated and experimentally obtained melting threshold of indium (in water) practically coincide, namely $E_{inc}$ = 80 mJ/cm$^2$.

## 4. Conclusions

This article shows that a shock wave in a solid during its formation and propagation as well as before its appearance leads to formation of dislocations due to gradual increase in the pressure gradient. The density of the dislocations increases with depth and is maximum at the site of the shock wave formation.

A method of nanosecond laser irradiation of In/CdTe structures in water with FTA control of *in-situ* pressure generation has been implemented. The frequency range of the recorded induced acoustic pulses is 20…2000 kHz.

It has been found out that the pressure value in the energy release region during irradiation of In/CdTe with a neodymium laser ($\tau_{pulse}$ = 7 ns) in water is 15…17 times greater than that during irradiation in air in the case of only the FTA signal. In the case of indium melting, the pressure value is 90…100 times greater.

It has been found out that the melting threshold at irradiation of In/CdTe in distilled deionized water with a neodymium laser ($\tau_{pulse}$ = 7 ns) is $E_{inc}$ = 80 mJ/cm$^2$, which is lower than that when irradiation takes place in air (115 mJ/cm$^2$). This is explained by the absence of indium ablation at these energies.

It has been found that at irradiation of In/CdTe in water, starting from an energy density $E_{inc}$ = 260 mJ/cm$^2$, the amplitude of the acoustic response sharply increases, which is accompanied by appearance of ablation traces (erosion craters) on the In surface, which depth reaches the CdTe surface. Therefore, irradiation with $E$ higher than $E_{inc}$ is impractical for effective doping.

The time-temperature profiles and the melt front speed $V$ during nanosecond laser irradiation of the In film (400 nm)/CdTe system have been calculated. $V$ has been found to vary from 5.47 to 80.6 m/s when $E_{inc}$ changes from 80 to 310 mJ/cm$^2$ and to have a close to logarithmic dependence. At such values of $V$, the additional pressure from melting becomes proportional to the photothermo-acoustic pressure.

The pressure control based on the induced acoustic response used in this work has made it possible to find the optimal interval of laser pulse energies (80…160 mJ/cm$^2$), at which effective diffusion of the impurity (In) is realized in the absence of intensive defect formation in CdTe during irradiation in water. The In/CdTe structures formed in this way have sharp rectifying properties.

## References


1. Levytskyi S.M., Gnatyuk D.V., Koba O.V. Mass transmission regularities in CdTe under nanosecond laser irradiation. *Phys. Chem. Solid State*. 2022. **23**. P. 150. https://doi.org/10.15330/pcss.23.1.150-153.
2. Baidullaeva A., Veleshchuk V.P., Vlasenko O.I. *et al.* Mechanisms of mass transfer of indium in CdTe under nanosecond laser irradiation. *Ukr. J. Phys*. 2011. **56**, No 2. P. 168–174. https://doi.org/10.15407/ujpe56.2.168.
3. Zharov V.P., Letokhov V.S. *Laser Optoacoustic Spectroscopy*. Springer Series in Optical Sciences. Vol. 37. Springer, Berlin, Heidelberg, 1986. https://doi.org/10.1007/978-3-540-39492-1.
4. Sklyarchuk V., Gnatyuk V., Aoki T. Effect of the metal nature on the I-V characteristics of CdTe diodes for ionizing radiation detectors. *Proc. SPIE*. 2023. **12696**. P. 126960L-1. https://doi.org/10.1117/12.2676538.
5. Hatanaka Y., Niraula M., Aoki Y. *et al.* Surface processing of CdTe compound semiconductor by excimer laser doping. *Appl. Surf. Sci*. 1999. **142**. P. 227–232. https://doi.org/10.1016/S0169-4332(98)00657-6.
6. Nishizawa J., Miyake T., Takagi T. *et al.* Resistance to pressure in laser-doped *p-n* and Schottky-type barrier junctions. *Sens. Mater*. 2024. **36**, No 1. P. 209–215. https://doi.org/10.18494/SAM4670.
7. Gnatyuk V.A., Aoki T., Vlasenko O.I. *et al.* Modification of the surface state and doping of CdTe and CdZnTe crystals by pulsed laser irradiation. *Appl. Surf. Sci*. 2009. **225**, No 24. P. 9813. https://doi.org/10.1016/j.apsusc.2009.04.096.
8. Owens A., Peacock A. Compound semiconductor radiation detectors. *Nucl. Instrum. Meth. Phys. Res. A*. 2004. **531**. P. 18. https://doi.org/10.1016/j.nima.2004.05.071.
9. Levytskyi S.M., Zhao T., Cao Z., Stronski A.V. Modeling of diffusion motion of nanoparticles in a CdTe crystal during laser-induced doping. *Phys. Chem. Solid State*. 2021. **22**, No. 2. P. 301–306. https://doi.org/10.15330/pcss.22.2.301-306.
10. Gnatyuk V.A., Aoki T., Hatanaka Y. Laser-induced shock wave stimulated doping of CdTe crystals. *Appl. Phys. Lett.* 2006. **2**, No 24. P. 242111. https://doi.org/10.1063/1.2213511.
11. Aoki T., Gnatyuk D.V., Levytskyi S.N. *et al.* Influence of nanosecond laser irradiation on optical properties of surface layers of CdTe crystals. *Thin Solid Films*. 2011. **519**, Issue 9. P. 2834–2837. https://doi.org/10.1016/j.tsf.2010.12.049.
12. Gnatyuk V. In/CdTe/Au *p-n* junction-diode X/γ-ray detectors formed by frontside laser irradiation doping. *Nucl. Instrum. Meth. Phys. Res. A*. 2022. **1029**. P. 166397. https://doi.org/10.1016/j.nima.2022.166397.
13. Levytskyi S., Cao Z., Koba A., Koba M. Dependence of the melting threshold of CdTe on the wavelength and pulse lifetime of laser radiation. *Mater. Rep*. 2024. **38**, No 7. P. 22120127 (1–6). https://doi.org/10.11896/cldb.22120127.

14. Hosoya N., Nagata M., Kajiwara I. Acoustic testing in a very small space based on a point sound source generated by laser-induced breakdown: stabilization of plasma formation. *J. Sound Vib.* 2013. **332**. No 19. P. 4572–4583. https://doi.org/10.1016/j.jsv.2013.03.035.
15. Veleschuk V.P., Vlasenko A.I., Gatskevich E.I. *et al.* Doping of cadmium telluride by indium at nano-second laser irradiation of In/CdTe structure. *J. Mater. Sci. Eng. B.* 2012. **2**, No 4. P. 230-239.
16. Meyer J.R., Kruer M.R., Bartoli F.J. Optical heating in semiconductors: Laser damage in Ge, Si, InSb, and GaAs. *J. Appl. Phys.* 1980. **51**, No 10. P. 5513–5521. https://doi.org/10.1063/1.327469.
17. Medvid' A., Mychko A., Gnatyuk V. *et al.* Mechanism of nano-cone formation on $Cd_{0.9}Zn_{0.1}Te$ crystal by laser radiation. *Opt. Mater.* 2010. **32**, No 8. P. 836. https://doi.org/10.1016/j.optmat.2010.03.006.
18. Hrdlička A., Zaorálková L., Galiová M. *et al.* Correlation of acoustic and optical emission signals produced at 1064 and 532 nm laser-induced breakdown spectroscopy (LIBS) of glazed wall tiles. *Spectrochim. Acta B.* 2009. **64**, Issue 1. P. 74–78. https://doi.org/10.1016/j.sab.2008.10.043.
19. Fincke J.R., Wynn C.M., Haupt R. *et al.* Characterization of laser ultrasound source signals in biological tissues for imaging applications. *J. Biomed. Opt.* 2018. **24**, No 2. P. 021206. https://doi.org/10.1117/1.JBO.24.2.021206.
20. Veleschuk V.P., Gnatyuk V.A., Aoki T. *et al.* Melting threshold and thermal conductivity of CdTe under pulsed laser irradiation, in: A.R. Varkonyi-Koczy (Ed.) Engineering for Sustainable Future. INTER-ACADEMIA 2019. *Lecture Notes in Networks and Systems*, **101**. Springer, Cham, 2020. https://doi.org/10.1007/978-3-030-36841-8_10.
21. Aoki T., Gnatyuk V.A., Vlasenko O.I., Levytskyi S.N. Formation of CdTe diode detectors by laser irradiation in water, in: *IEEE Nuclear Science Symposium & Medical Imaging Conference*, Knoxville, TN, USA, 2010. P. 3785–3788. https://doi.org/10.1109/NSSMIC.2010.5874520.
22. Madelung O. *Semiconductors: Data Handbook*. Springer, 2004.
23. Gnatyuk V.A., Aoki T., Niraula M., Hatanaka Y. Influence of laser irradiation and laser-induced In doping on the photoluminescence of CdTe crystals. *Semicond. Sci. Technol.* 2003. **18**. P. 560. https://doi.org/10.1088/0268-1242/18/6/329.
24. Triboulet R., Siffert P. (Eds.) *CdTe and Related Compounds; Physics, Defects, Hetero- and Nano-structures, Crystal Growth, Surfaces and Applications*. Elsevier, 2010.

**Author and CV**

**Levytskyi Serhii M.,** PhD, Senior Researcher at the Department of Optoelectronics, V. Lashkaryov Institute of Semiconductor Physics, NAS of Ukraine. Author of more 150 publications and 6 patents. Field of research: technologies of synthesis of II-VI and IV-VI semiconductors; experimental and theoretical investigation of photoelectric, electrical, optical and structural properties of these semiconductors, nanosecond laser processing, laser-induced doping of CdTe metal-semiconductor contacts and diode structures, as well as IR and X/γ-ray detectors.
http://orcid.org/0000-0002-3909-0993

**Термодинамічні та кінетичні процеси модифікування гетеросистем на основі телуриду кадмію, ініційовані наносекундною дією інтенсивного лазерного випромінювання**

**С.М. Левицький**

**Анотація.** У роботі розглянуто механізми масопереносу в системі In/CdTe при наносекундному імпульсному лазерному опроміненні, які зумовлені нестаціонарністю, нерівноважністю, фізичною та геометричною нелінійністю, високою швидкістю і одночасністю протікання різних фізичних процесів, а також проаналізовано порогові процеси – фазові переходи, абляція у гетеросистемі метал/CdTe при потужному наносекундному лазерному опроміненні за нормальних умов та у рідкому середовищі. Установлено пороги плавлення та абляції при наносекундному лазерному опроміненні структур плівка металу (In)/CdTe у воді та вивчено їх зміну від виникнення нелінійностей (за рахунок зміни фізичних параметрів In) і генерації тиску. Установлено, що величина тиску в області енерговиділення при опроміненні In/CdTe неодимовим лазером ($\tau_{імп}$ = 7 нс) у воді в 17 раз більша у випадку фототермоакустичного ефекту та у 90 раз більша у випадку плавлення індію.

**Ключові слова:** CdTe, In/CdTe, імпульсне лазерне опромінення, легування, фототермоакустичний ефект, плавлення.